Applied Thermal Engineering 213 (2022) 118724

Contents lists available at ScienceDirect

Applied Thermal Engineering

journal homepage: www.elsevier.com/locate/apthermeng

Research Paper

Computational fluid dynamic study on the adsorption-based desalination and cooling system

Mingliang Li, Yanan Zhao, Rui Long *, Zhichun Liu, Wei Liu

School of Energy and Power Engineering, Huazhong University of Science and Technology, Wuhan 430074, PR China

ARTICLE INFO

Keywords:
Adsorption desalination
Fin shape
CFD model
Machine learning
Water production

ABSTRACT

Adsorption desalination (AD) is a potentially competitive alternative for potable water production. Unlike traditional rectangular fins for finned-tube adsorbent bed in the AD system, in this study, bullet- and umbrella-shaped fins are employed in the adsorbent bed to improve the heat and mass transfer characteristics in the adsorption/desorption processes, thus augmenting the system performance. Based on a complete transient mathematical model incorporating a three-dimensional computational fluid dynamic model for adsorber and lumped models for evaporator and condenser, impacts of fin configurations regarding base diameter, tip diameter, and shape factor on system performances considering the adsorbent and the whole bed are comprehensively analyzed. Results reveal that a larger base and tip diameter with a lower shape factor contribute to specific bed productions. The underlining relationship between fin configurations and overall performance (total daily water production, total cooling power, and coefficient of performance) is further explored via machine learning. And the optimal fin shape is identified by the genetic algorithm. The optimal base diameter, tip diameter, and shape factor are 0.262, 0.517, and 4.20, respectively, which render a total water production of 5.20 m^3/day with a total cooling power of 0.149 kW and coefficient of performance of 0.855.

Nomenclature

A	Area	m^2
C_p	Specific heat	J kg^{-1} K^{-1}
COP	Coefficient of performance	–
d_p	Particle diameter	m
d_{tip}	Tip diameter	mm
D	Base diameter	mm
D_s	Mass diffusivity	m^2 s^{-1}
D_{so}	Pre-exponential factor	m^2 s^{-1}
E	Characteristic energy	J mol^{-1}
E_a	Activation energy	J mol^{-1}
F	Fin thickness	mm
H	Bed height	mm
H_a	Heat of adsorption	J kg^{-1}
h_{fg}	Latent heat of vaporization	J kg^{-1}
h	Convective heat transfer coefficient	W m^{-2} K^{-1}
i	Flag describing different cycle phases	–
K	Permeability	m^2
k	Thermal conductivity	W m^{-1} K^{-1}
L	Model length	mm
L_0	Total tube length	mm
L_1	Length of discontinuous fin	mm
l	Coefficient associated with the fin shape	mm

(*continued on next column*)

Nomenclature (*continued*)

M	Mass	kg
$\dot{m}$	Mass flow rate	kg/s
n	Surface heterogeneity factor	–
n_{fin}	Number of fins	–
P	Pressure	Pa
Q	Heat	J
R	Universal gas constant	J mol^{-1} K^{-1}
R_0	Inner tube radius	mm
S	Salinity	–
SCP	Specific cooling power	kW kg^{-1}
SDWP	Specific daily water production	m^3 ton^{-1} day^{-1}
T	Temperature	K
TCP	Total cooling power	kW
TDWP	Total daily water production	m^3 day^{-1}
t	Time	s
U	Overall heat transfer coefficient	W m^{-2} K^{-1}
$\vec{U}$	Velocity vector	m s^{-1}
W	Water uptake	kg kg^{-1}
W_∞	Maximum adsorbent capacity	kg kg^{-1}
W_o, W^*	Equilibrium uptake	kg kg^{-1}
Greek Symbols		
ε	Porosity	–

(*continued on next page*)

* Correspondence author.
E-mail address: r_long@hust.edu.cn (R. Long).

https://doi.org/10.1016/j.applthermaleng.2022.118724
Received 20 February 2022; Received in revised form 2 May 2022; Accepted 21 May 2022
Available online 27 May 2022

Nomenclature (*continued*)

μ	Dynamic viscosity	Pa s
ρ	Density	kg m^{-3}
α	Thermal diffusivity,	m^2 s^{-1}
Subscripts		
a	Adsorbent	
av	average	
ads	Adsorption	
b	Bed	
c	Cooling, condenser	
ch	Chilled water	
con	Condenser	
cw	Cooling water	
cycle	Cycle time	
des	Desorption	
eva	Evaporation	
eff	Effective	
e	Evaporator	
f	Fluid	
h	Heating	
Hex	Heat exchanger	
ini	Initial	
p	Particle	
s	Saturation, solid	
sg	Silica gel	
sw	Seawater	
sat	saturation	
S	Salinity	
t	Total	
v	Vapor phase	
w	Water	

1. Introduction

In the past few decades, scarcity of potable water around the world has increasingly menaced human survival, especially in the desert and semi-arid regions. Drinking water is an indispensable resource for economic development and human consumption, as it is needed in agriculture, industry, and domestic applications.

As the limitation of total natural freshwater resources which accounts for merely 3% of the water on earth, seawater desalination is extremely emphasized, which can ease the shortage of natural potable water via the desalination of abundant seawater or brackish water at the cost of energy consumption. Traditionally commercially utilized desalination technologies are as follows: i) reverse osmosis (RO) [1], a technology producing potable water via a semipermeable membrane through which merely the water molecules can get through; ii) multi-stage flash (MSF) [2] which is considered the most mature desalination technology and accounts for 64% of the total; iii) multi-effect distillation (MED) [3], occupying 9% of the desalinated water and consuming the thermal energy; iv) electro-dialysis (ED) [4]. However, they suffer from shortcomings consisting of equipment maintenance, high cost, and a large amount of energy consumption. Alternative desalination technologies driven by renewable energy [5] or low-grade heat sources are appealing [6]. Adsorption desalination (AD) [7–9], utilizing low-grade heat such as waste heat [10] and solar energy [11] to actuate the desorption of water vapor in the hydrophilic porous material, has obtained particular interest. It can produce desalinated water as well as provide refrigeration, which is extraordinarily suitable for the semi-arid area to store medicine and essentials for survival [12].

The AD system has proved to be an energy-efficient [13] and environmentally friendly method [14,15], which contains three major components: adsorber, evaporator, and condenser, as presented in Fig. 1. The AD cycle can be sub-categorized into the adsorption-evaporation and the desorption-condensation phase [16]. During the former phase, seawater is pumped to the evaporator, vaporizing and being adsorbed by the adsorbent particles. Water is separated from salt and refrigeration is produced during the evaporation. The latter phase is dedicated to producing potable water, in which the vapor inside particle pores is liberated under heating and then condenses inside the condenser.

Conventional models employed to describe the AD system are the lumped (LP) model [17] and the computational fluid dynamics (CFD) model [18,19]. The former is usually used for cycle simulation, which regards the bed as temperature and pressure uniform, and fails to investigate the local bed heat and mass transfer characteristics that can be revealed by employing the CFD model [20]. High heat and mass transfer resistance inside porous media hinders the commercialization of AD technology [21]. Many efforts have been dedicated to improving the system performance: i) system optimization with respect to more appropriate operation conditions such as the cycle time allocation [22], the complicated system incorporating several beds and multiple stages [23,24], and the extra heat recovery pipe to elevate the evaporator pressure and the energy efficiency [25,26], where LP model is generally utilized and the particular heat and mass transfer characteristics in the bed are not considered; ii) investigation dedicated to improving heat and mass transfer performance in the adsorbent bed [27], where the CFD model is employed to describe the spatial distribution of the physical quantities in the bed; iii) exploration on the dynamics of new adsorbent possessing the better thermodynamic properties such as the metal organic framework (MOF) [28,29]; iv) particle level study on the loose grain configuration and adsorption model [30,31]. Ilis et al. [32] examined an annular adsorber with radial fins and found that enhancement of heat transfer via adding fins is obvious only if the thermal diffusivity ratio and fin coefficient are low enough. Niazmand et al. [33] explored the heat and mass transfer in a cylindrical bed with annular fins via a transient two-dimensional numerical model. The effects of bed configurations consisting of fin pitch, bed height, and particle size on the system performance were examined. At a slight cost of lower coefficient of performance (COP), the insert of fins can elevate the cooling power dramatically. They further [27] employed a three-dimensional and non-equilibrium numerical model to derive the combined heat and mass transfer characteristics in a bed with plate fins. The effects of fin spacing and height on the COP were investigated. Kowsari et al. [34] investigated the geometrical configuration of a finned flat-tube bed using a transient three-dimensional CFD model, revealing that the heat transfer resistance was significantly impacted by the fin pitch and height. Saleh et al. [35] investigated the performance of an adsorbent bed using wire finned heat exchanger compared to the rectangular and microchannel heat exchanger in an adsorption heat pump using aluminum fumarate which belongs to the MOF material. The microchannel bed presented large mass resistance that was almost five times higher than the other studied fins, while the wire finned bed presented a superior cooling performance. Li et al. [36] investigated the effect of ununiform porosity distribution on the system cooling effect and water production via an two-dimensional CFD axisymmetric model along with the time-dependent evaporator pressure. The bed configurations incorporating fin shape and the operating conditions were examined. Later, the effects of two field synergy parameters reflecting the heat and mass transfer characteristics in a finned-flat bed of the AD system were explored [37]. An alternative method to evaluate the heat and mass transfer performance inside the adsorbent bed was established. Mahmoud et al. [38] established a detailed CFD model along with a non-ideal evaporator and condenser, and the operation conditions and fin configurations were investigated.

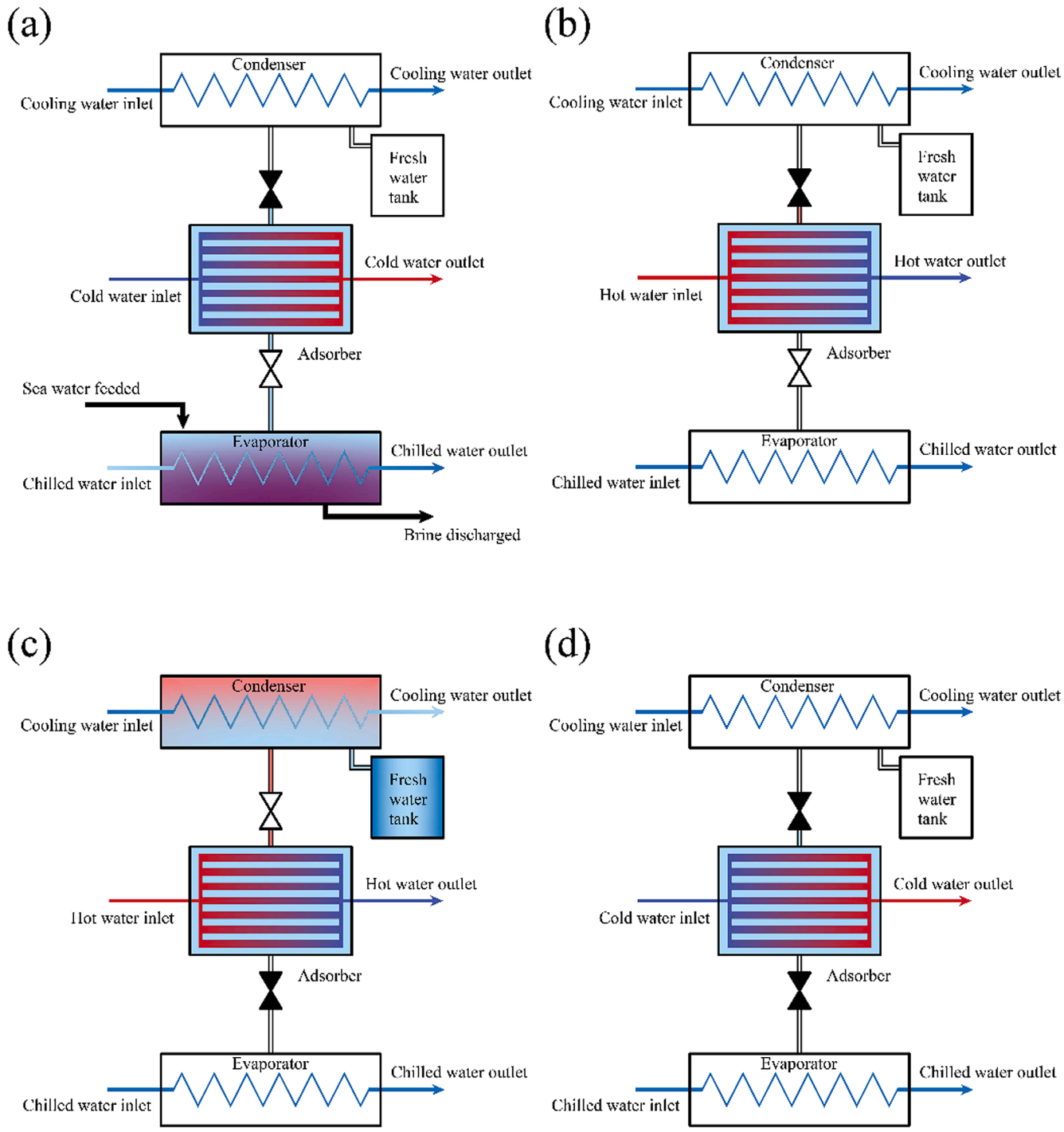

Fig. 1. Schematic of the AD system, (a) the adsorption process, (b) the preheating process, (c) the desorption process, and (d) the precooling process.

For a finned-tube adsorbent bed in the AD system, the fin configurations in previous literature are mainly focused on rectangular fins, which may be not the most suitable for the application of the AD system. Thus, the study dedicates to fin configurations with irregular shapes. In order to achieve this purpose, a mathematical function with three parameters is employed to control the fin edge establishing bullet- or umbrella-shaped fins. Based on a complete transient mathematical model that incorporates a three-dimensional computational fluid dynamic model for adsorbent bed and lumped models for evaporator and condenser, the effects of fin configurations regarding base diameter, tip diameter, and shape factor on system performances considering the adsorbent and the whole bed are comprehensively analyzed. Ensemble-based machine learning is employed to reveal the underlining quantitative relationship between fin configurations and the overall performance of the AD system (total daily water production, total cooling power, and COP). Based on the obtained relationship revealed by machine learning, the optimal fin configurations are further identified via the genetic algorithm. And the impacts of the discontinuous fin configuration are also explored.

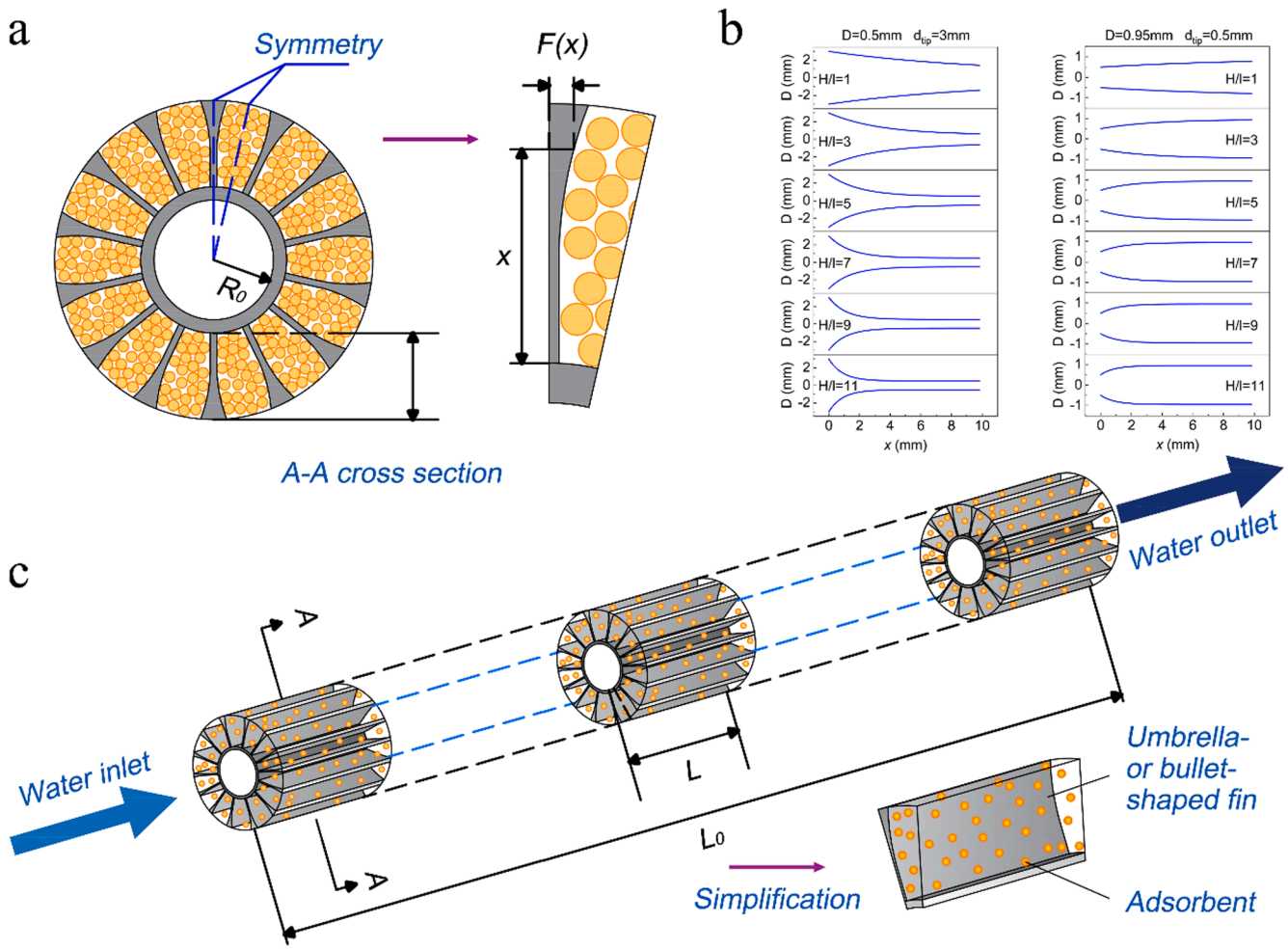

Fig. 2. (a) Schematic of the cross-sectional view of the implemented adsorber. (b) Variations of the umbrella-or bullet-shaped fin edge with the factor *H/l*. (c) Profile of the 3D view of the finned-tube bed.

2. System description

As presented in Fig. 2(a) and (c), a radial bullet- or umbrella-shaped finned-tube adsorbent bed is investigated, where n_{fin} is the number of fins, L_0 the total tube length, R_0 the tube inner radius, H the bed height. Loose particles are filled between the adjacent fins, being cooled or heated by the water flowing inside the tube. The values of bed geometrics have been listed in Table 2. The total tube length L_0 is used to calculate the overall production as the adsorbent mass needs to match the evaporator and condenser parameters while L is the practical model length involved in the CFD simulation.

2.1. Assumptions and simplifications

The following assumptions and simplifications have been adopted in the modeling [26,39]:

1. The adsorbent particles are ideal spheres with constant diameter.
2. The vapor and liquid of adsorbate is an ideal gas and liquid phase.
3. The adsorption kinetics can be imitated by a linear driving force model while the pressure drop is simulated via Darcy's law.
4. The local thermal equilibrium assumption can be employed in the bed.
5. Physical properties of solid materials can be calculated as constant, latent heat of evaporation is invariant with temperature and salinity.
6. Fluctuations of the cooling and heating temperature can be neglected, the convective heat transfer coefficient is constant [40].
7. The spatial temperature and pressure inside the evaporator and condenser are invariant, hence it can be captured via a lumped model.
8. The contact resistance between the adsorbent particles and the solid fins is not considered and is neglected. And the boundary condition is assumed to be constant in the bed length direction thus the channel pitch is ignored [34,39].

2.2. Mathematical modeling

The numerical modeling details of all the components involved have been presented in Table 1. The evaporator and condenser are considered to be lumped, here $M_{sw,eva}$ is the mass of seawater in the evaporator, $M_{w,con}$ the mass of desalinated water in the condenser, M_{sg} the silica gel mass, i the flag describing different cycle phases ($i = 1$ for adsorption and desorption, $i = 0$ for precooling and preheating). The seawater constantly vaporizes under the effect of hydrophilic porous adsorbent hence the reduction of water mass is equal to the net uptake of the bed. In the energy balance equation, $(MC_p)_{Hex,eva}$, $(MC_p)_{Hex,con}$, $(MC_p)_{sw,eva}$, and $(MC_p)_{w,con}$ are the thermal masses of the heat exchanger of evaporator and condenser and the thermal masses of seawater and desalinated water, h_{fg} the latent heat of evaporation, $m_{ch,eva}$, $m_{cw,con}$, $C_{p,ch}$, $C_{p,cw}$, $T_{ch,in}$, $T_{cw,in}$, $T_{ch,out}$, and $T_{cw,out}$ are the mass flow rate, heat capacity, inlet

Table 1
A summary of mathematical modeling involved in the study.

Components	Balance equation	Expression
Evaporator [25,41]	Mass balance	$\frac{dM_{sw,eva}}{dt} = -iM_{sg}\frac{dW_{ads}}{dt}$
	Energy balance	$[(MC_p)_{Hex} + (MC_p)_{sw}]^{eva}\frac{dT_{eva}}{dt} = -nh_{fg}M_{sg}\frac{dW_{ads}}{dt} + \dot{m}_{ch,eva}C_{p,ch}(T_{ch,in} - T_{ch,out})^{eva}$
	Outlet water temperature	$T_{ch,out} = T_{eva} + (T_{ch,in} - T_{eva})\exp\left(\frac{-UA_{eva}}{m_{ch,eva}C_{p,ch}}\right)$
	Evaporator pressure	$P_{eva} = (1 - 0.537S)P_{sat}$
	Saturated pressure [42]	$P_{sat} = 8.143 \times 10^{10}\exp(-5071.7/T_{eva})$
Condenser	Mass balance	$\frac{dM_{w,con}}{dt} = -nM_{sg}\frac{dW_{des}}{dt}$
	Energy balance	$[(MC_p)_{Hex} + (MC_p)_w]^{con}\frac{dT_{con}}{dt} = nh_{fg}M_{sg}\frac{dW_{des}}{dt} + \dot{m}_{cw,con}C_{p,cw}(T_{cw,in} - T_{cw,out})^{con}$
	Outlet water temperature	$T_{cw,out} = T_{con} + (T_{cw,in} - T_{con})\exp\left(\frac{-UA_{con}}{m_{cw,con}C_{p,cw}}\right)$
Adsorber	Adsorption isotherm (D-A equation) [40]	$W_o = W_\infty\exp(-(\frac{RT}{E}\ln(\frac{P_s}{P}))^n)$
	Adsorption kinetics (LDF model)	$\frac{\partial W}{\partial t} = \frac{60D_s}{d_p^2}(W_o - W)$
	Pressure drop (Darcy's law)	$\vec{U} = -\frac{K}{\mu}\nabla P$
	Mass balance [43,44]	$\frac{\partial(\varepsilon_b\rho_v)}{\partial t} + \nabla.(\rho_v\vec{U}) + \rho_b\frac{\partial W}{\partial t} = 0$
	Energy balance [45]	$(\varepsilon_b\rho_vC_{pv} + \rho_b(C_{ps} + WC_{pw}))\frac{\partial T}{\partial t} + \rho_vC_{pv}\vec{U}\cdot\nabla T = \nabla\cdot(k_{eff}\nabla T) + \rho_bH_a\frac{\partial W}{\partial t}$
	Heat conduction [46,47]	$\frac{\partial T}{\partial t} = \alpha\nabla^2T$
	D_s the surface diffusivity	$D_s = D_{so}\exp(-\frac{E_a}{RT})$
	K the bed permeability	$K = \frac{d_p^2\varepsilon_b^3}{150(1-\varepsilon_b)^2}$
Cycle control [48,49]	W_{min}	$W_{\min} = W^*_{\min} + 0.35(W^*_{\max} - W^*_{\min})$
	W_{max}	$W_{\max} = W^*_{\max} - 0.2(W^*_{\max} - W^*_{\min})$
System performance	SDWP	$SDWP = \frac{-\Delta W_{av,des}}{\rho_w t_{cycle}}$
	SCP	$SCP = \frac{h_{fg}\Delta W_{av,ads}}{t_{cycle}}$
	TDWP	$TDWP = M_{sg}\frac{-\Delta W_{av,des}}{\rho_w t_{cycle}}$
	TCP	$TCP = M_{sg}\frac{h_{fg}\Delta W_{av,ads}}{t_{cycle}}$
	COP	$COP = M_{sg}\frac{h_{fg}\Delta W_{av,ads}}{Q_{des} + Q_h}$
Fin	Shape control	$F(x) = D - (D - d_{tip})\exp(-x/l)$

and outlet temperature of the chilled water and cooling water. The left term represents the temporal heat capacity of the two heat exchangers, while the first and second terms on the right indicate the latent heat of evaporation or condensation and the sensible heat from temperature fluctuation of chilled water or cooling water. The outlet water temperature can be estimated using the log mean temperature difference method, where UA_{eva} and UA_{con} are the overall heat transfer coefficient of the two heat exchangers. The evaporator pressure (P_{eva}) is calculated as a function of evaporator temperature (T_{eva}) and salinity (S) which is derived from the concentration balance, while the condenser pressure (P_{con}) can be captured merely by the temperature. Hence, the transient pressure and temperature in the two heat exchangers are commendably gained, subsequently, it is input to the CFD study as boundary conditions for the adsorber bed Fig. 3.

The D-A equation is used to capture the equilibrium uptake (W_o). Different from the Langmuir model, the D-A equation is derived from the micropore filling theory which is established based on the experimental fact that the adsorption capacity is related to the uptake on the surface of the adsorbent. Here W_∞ is the maximum uptake, R the universal gas constant, E the characteristic energy, n the heterogeneity factor, P_s the saturated pressure, P the temporal bed pressure, T the bed temperature. The adsorption or desorption rate is estimated via the equilibrium uptake and the kinetics which is captured by the linear driving force (LDF) model, where d_p is the particle diameter, W the transient uptake, and D_s the surface diffusivity which can be estimated by the pre-exponential factor (D_{so}) and the activation energy (E_a). The LDF model is frequently and successfully utilized in the simulation of gas adsorption dynamics due to its simple form and relatively favorable accuracy. The pressure drop is described by employing Darcy's law since the inertial term and viscosity term can be neglected at such a low fluid velocity through the flexural gap between adsorbent particles. Here μ is the vapor viscosity, K the bed permeability which can be expressed by the particle diameter (d_p) and the bed porosity (ε_b), and U the vapor velocity vector which can be captured by the mass balance equation, where ρ_v and ρ_b are the density of vapor and bed. The transient bed temperature is derived from the energy balance equation, where C_{pv}, C_{ps}, and C_{pw} are the heat capacity of vapor, adsorbent, and water, k_{eff} the effective heat conductivity, H_a the enthalpy of adsorption. The heat conduction through the radial fins is captured by the thermal differential equation where α is the thermal diffusivity of metal material. The fundamental parameters of the selected evaporator/condenser and the thermophysical and dynamical characteristics of the silica gel RD type are presented in

Table 2
The values involved in the modeling [22,51].

Parameter	Value
n_{fin}	14
L_0	1 m
L	20 mm
R_0	12.85 mm
H	9.85 mm
$C_{p,s}$	924 kJ K/kg
E_a	42000 J/(mol K)
D_{so}	2.54×10^{-4} m^2/s
ρ_b	740 kg/m^3
d_p	0.35 mm
ε_b	0.37
k_b	0.198 W K/m
H_a	2415 kJ/kg
W_∞	0.37 kg/kg
E	4280 J/mol
n	1.15
T_{ini}	60℃
$T_{eva,ini}$	10℃
$M_{sw,ini}$	50 kg
$M_{w,ini}$	20 kg
$T_{ch,in}$	20℃
$T_{cw,in}$	20℃
T_h	75℃
T_c	30℃

Table 2.

The initial and boundary conditions are presented in Table 2, where R_0 and R are the outer radius of tube and bed, T_f, T_h, and T_c are the temperature of fluid, heating, and cooling. The durations of adsorption and desorption are manipulated by two equations depicted in Table 1, where W_{min} and W_{max} are the possible final equilibrium uptake for the adsorption and desorption phase, $W^*_{\min}$ and $W^*_{\max}$ are the equilibrium uptake under the condenser and evaporator pressure and the heating and cooling temperature. The parameters $W^*_{\min}$ and $W^*_{\max}$ represent the saturated uptake when the duration of desorption and adsorption is sufficiently long. W_{min} and W_{max} define the uptake when the adsorption and desorption phase end, the constant used in the expression has been comprehensively investigated in [50]. The coefficients in the expressions are determined from our previous study which elucidates its advanced system performance. Moreover, the preheating and precooling are ended while the pressure of the bed outer edge attains the transient condenser and evaporator pressure. The basic parameters of the evaporator and condenser, as well as the detailed initial values are listed in Table 2. The boundary conditions for each process can be found in our previous study [50].

The cyclic steady state can be achieved in 4–5 cycles after the commencement of calculation. Two indicators reflecting the adsorbent performance and three parameters considering the whole system are employed to estimate the operating status and throughput of the cycle: the specific daily water production (SDWP), the SCP, the total daily water production (TDWP), the total cooling power (TCP), and the COP. The expressions are listed in Table 1, where t_{cycle} is the cycle time which is calculated as the sum of the duration of the four processes manipulated by the cycle control condition listed in Table 1, ρ_w the water density, $\Delta W_{av,ads}$ and $\Delta W_{av,des}$ the working capacity during adsorption and desorption, Q_{des} and Q_h the total heat in the desorption and preheating process, which is calculated via the integral of heat flux over time. The COP is defined as the ratio of the cooling effect during adsorption to the total supplied heat during preheating and desorption processes in a complete steady cycle.

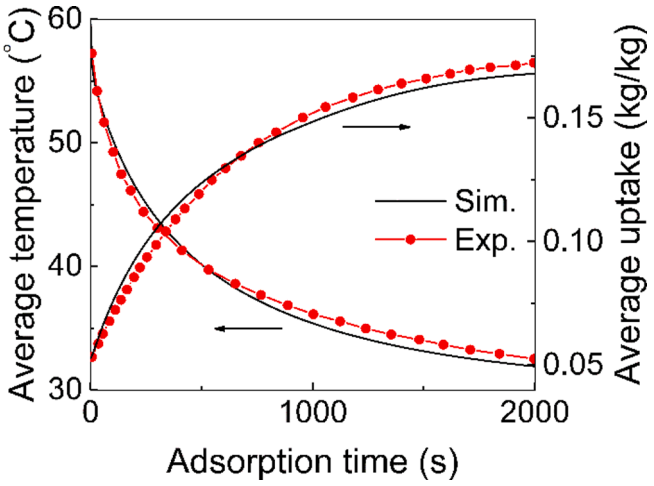

Fig. 3. Comparisons of temporal average temperature and uptake between the calculated results and experimental data from Ref. [52] and [53].

2.3. Mesh independence and model validation

The improved CFD model that includes the entire system incorporating a three-dimensional bed and lumped evaporator/condenser is solved via COMSOL Multiphysics. Transient average temperature and uptake in the adsorption with different configurations of mesh size and time step are compared to validate the grid dependence of the model. As listed in Table 3, a mesh size of 18,840 accompanied by a time step of 3 s is able to guarantee accurate and stable results. The calculated temporal temperature and uptake are validated by comparisons of the experimental data from Ref. [52] and Ref. [53]. It can be observed that the numerical results of transient uptake and temperature agree well with those of the experimental results, justifying the model employed in this study.

3. Results and discussion

Here, we employ bullet- or umbrella-shaped fins attached to the tube in the adsorption bed, thus improving the heat and mass transfer process in the adsorption/desorption process. The fine profile can be computed by a mathematical expression presented in Table 1, where F is the fin thickness, x the length along the centerline of each fin, d_{tip} the tip diameter, D the base diameter, l a parameter accounting for the curvature of the bullet- or umbrella-shaped outer fin edge, as presented in Fig. 2(b). For a small l with fixed D and d_{tip}, the fin thickness is constant at the base and top of the fin according to the expression. Changing l only affects the smoothness of the fin edge, thus the parameter l can be the coefficient associated with the fin shape. To make it dimensionless, the parameter H/l is defined as the shape factor controlling the smoothness of the fin edge. It can be observed from Fig. 2b that the larger shape factor leads to the slender fin root and causes the fin thickness to vary rapidly in the fin neck. The effects of the above three parameters manipulating the fin shape on system performance are systematically analyzed. Machine learning is employed to obtain the quantitative relationship between the three parameters and the total water production, which is then used for shape optimization via the genetic algorithm. In addition, the connection between the heat transfer enhancement and reduction of adsorbent mass derived from an exploration of the effect of discontinuous fin on cooling and water

Table 3
Variations of temperature and uptake with the mesh size and time step.

Time step	2 s				3 s			
Mesh size	18,840		42,400		18,840		42,400	
Time	W_{av}	T_{av}	W_{av}	T_{av}	W_{av}	T_{av}	W_{av}	T_{av}
150	0.1284	321.07	0.1283	321.07	0.1284	321.06	0.1283	321.08
300	0.1590	316.16	0.1589	316.16	0.1590	316.16	0.1589	316.17
450	0.1820	313.01	0.1820	313.02	0.1820	313.01	0.1819	313.02

desalination is also discussed.

3.1. Adsorbent consideration

To explore the effect of three fin shape parameters on heat and mass transfer characteristics in the radial finned-tube bed, the adsorbent indicators consisting of transient temperature and uptake, cycle time, SCP and SDWP are investigated.

3.1.1. The effect of base diameter

The temporal performances considering the adsorbent under three different base diameters are compared in Fig. 4. The tip diameter is fixed at 1 mm and the shape factor is set at 11. There exist large deviations in terms of average temperature and uptake between the three selected bed configurations, which demonstrates that the increase of base diameter results in an enhancement of cooling and uptake. These effects on bed adsorption can be attributed to the following reason: The augmentation of base diameter compresses the volume of the region that fills with the porous adsorbent possessing poor thermal conductivity hence it facilitates the heat transfer performance in the whole bed, which leads to the latent adsorbent heat quickly liberated. Consequently, the temperature is lowered, resulting in the adsorption phase being promoted and a larger uptake, which accounts for the temperature and uptake profile depicted in Fig. 5.

Based on the definition of SCP listed in Table 1, the increase of adsorption uptake due to the augment of base diameter leads to the SCP monotonically increasing, as shown in Fig. 6(a). The productions of cooling effect and desalinated water for adsorbent per unit weight and the cycle time with various base diameters and three fixed tip diameters are presented in Fig. 6(a), (b), and (c). As the cycle control conditions are calculated using the temperature and pressure boundary which is constant for all the configurations, the working capacity is nearly the same thus the variation of cycle time generally reflects the throughput. Moreover, a system reaching the cyclic steady state must ensure that the capacity during adsorption and desorption is approximately consistent, which leads to the qualitative behavior of cooling and water production being just alike. The accelerated adsorption and desorption kinetics due to the increase of base diameter and the enhancement of heat transfer results in a reduction of cycle time hence an augmentation of SCP and SDWP. Since the tip diameter and shape factor are fixed, a larger base diameter reduces the distance between fin roots, thus dramatically enhancing the heat transfer process in the regions adjacent to the tube wall where the temperature is lower and the adsorption is facilitated, as presented in Fig. 5. The improvement of heat transfer promotes the adsorption and desorption process, thus the system shows a shorter cycle time and higher specific cooling and water production.

3.1.2. The effect of tip diameter

As presented in Fig. 6, the larger base and tip diameter simultaneously lead to an improvement in system performance incorporating cooling and water production. Fig. 7 elucidated that the increase of tip diameter accounts for a lower bed temperature thus an augmentation of adsorption uptake. As presented in Fig. 8(a) and (b), the high-temperature region in the bed is extremely compressed, which is substituted by a well-enhanced heat transfer area adjacent to the fin surface, leading to the reduction of bed average temperature and the increase of uptake.

As shown in Fig. 9 the SCP and SDWP increase monotonously along with the increase of tip diameter due to the reduction of cycle time. The enhancement of heat transfer accelerates the adsorption process, leading to a shorter cycle time with nearly the same working capacity thus increasing the system throughput. The SCP varies from 0.303 kW/kg to 0.383 kW/kg for the base diameter in the range of 0.2–0.95 mm, which accomplishes around 26.4% of improvement, while 13.1% of elevation is observed by tip diameter augmentation from 0.5 mm to 3.0 mm. It illustrates that adjusting base diameter is more effective for enhancing the production of cooling and potable water. With fixed base diameter and shape factor, increasing the tip diameter effectively shortens the pitch between fin tips, which strengthens the heat transfer in the external regions. It leads to the lower temperature and larger uptake presented in Fig. 8, thus the system throughput per unit adsorbent mass is elevated.

3.1.3. The effect of shape factor

Fig. 8 depicts the transient average temperature and uptake in the adsorption under three different shape factors. It should be emphasized that when the H/l is at a fairly low stage ($H/l = 1$), the expression manipulating the fin outer edge may induce some problems, as the base diameter is calculated at $x = L$. A sufficiently large fin shape factor makes the index term in the calculation formula on the verge of 0 thus the base diameter is equal to the parameter D, while a low H/l leads to the base diameter in a bullet-shaped fin ($D > d_{tip}$) lower and in an umbrella-shaped fin ($D < d_{tip}$) larger. This discrepancy can be expressly observed in Fig. 12, where the temperature and uptake profiles for the cross-sectional bed plain with fin dimensions of $D = 0.5$ mm, $d_{tip} = 2$ mm, and $H/l = 1, 5, 11$ are presented. The base diameter for the bed with H/l fixed at 1 is distinctly shortened, compared with that of $H/l = 5$ and $H/l = 11$. The increase in base diameter improves the adsorbent performance. Moreover, the augment of shape factor leads to the cycle deteriorating, which can be elucidated in Fig. 10, as the bed with a shape factor of 11 has a higher temperature and lower adsorption uptake than that of $H/l = 5$. Besides, both the two factors are large enough to ensure a consistent base diameter. Consequently, when changing H/l to 1 for umbrella-shaped fins, the increase of base diameter and the reduction of shape factor simultaneously result in an improvement in system performance. As shown in Fig. 11 and Fig. 12, a larger shape factor leads to an increased cycle time and deteriorated cooling effect and water production. It can be attributed to the fact that a tortuous fin edge at a larger shape factor results in an augmentation of the adsorbent mass between adjacent two fins, which induces a poor heat transfer performance,

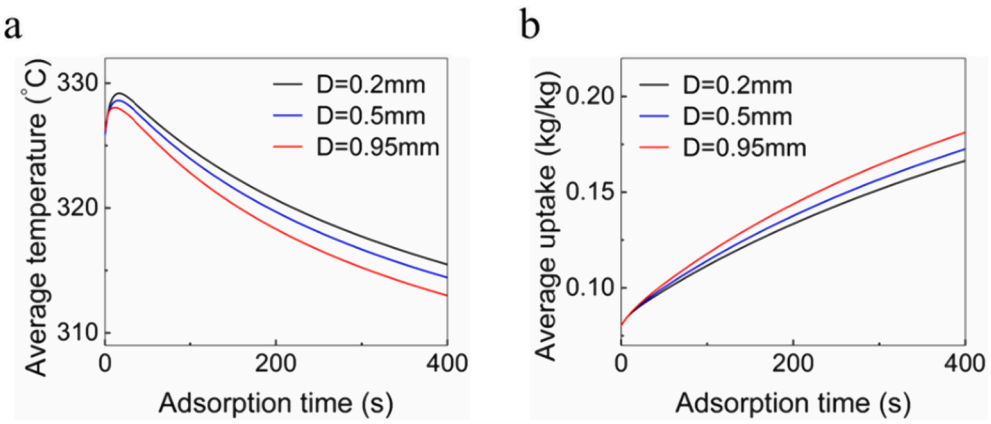

Fig. 4. Variations of (a) average temperature and (b) average uptake with adsorption time for different base diameters.

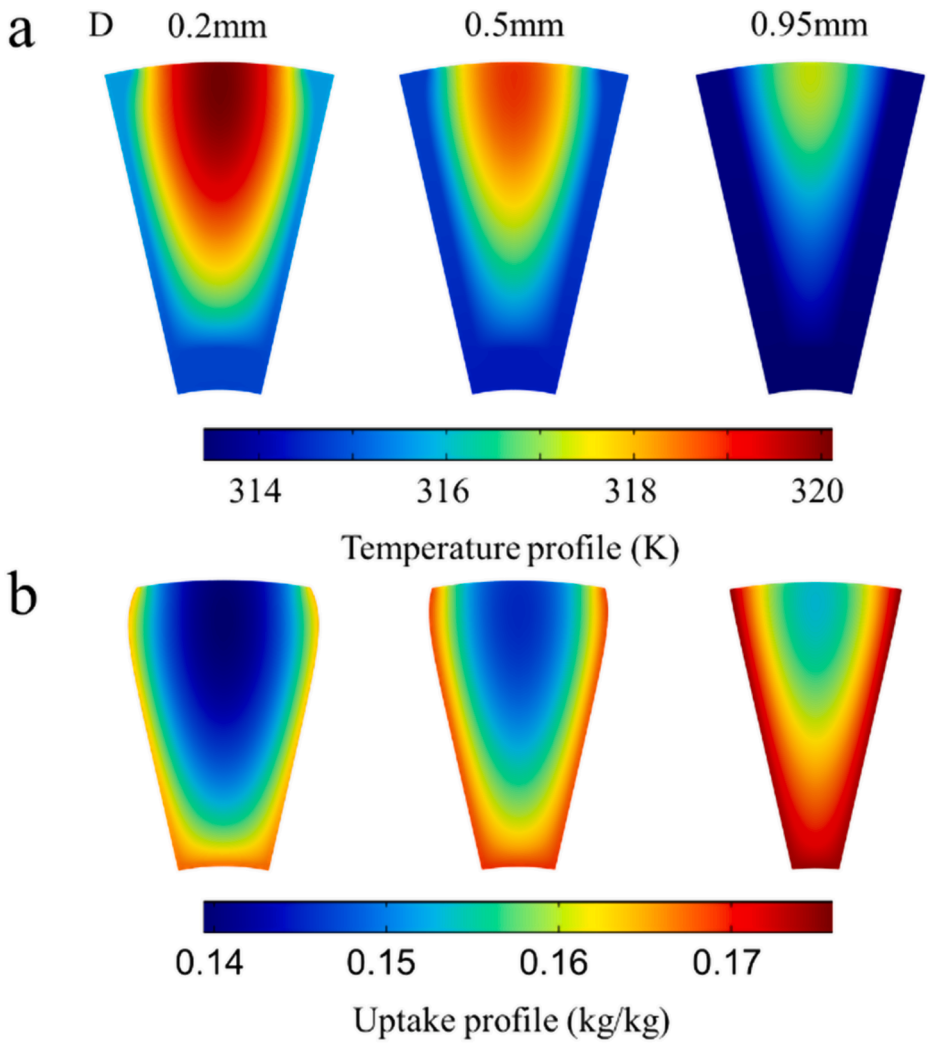

Fig. 5. (a) Temperature and (b) uptake distributions for the cross-sectional bed plain (the cross-section 10 mm from the surface) with fin dimensions of $d_{tip} = 1$ mm, $H/l = 11$ and $D = 0.2$ mm, 0.5 mm, 0.95 mm at 300 s of the isobaric adsorption process.

a-
u-
g-
m-
e-

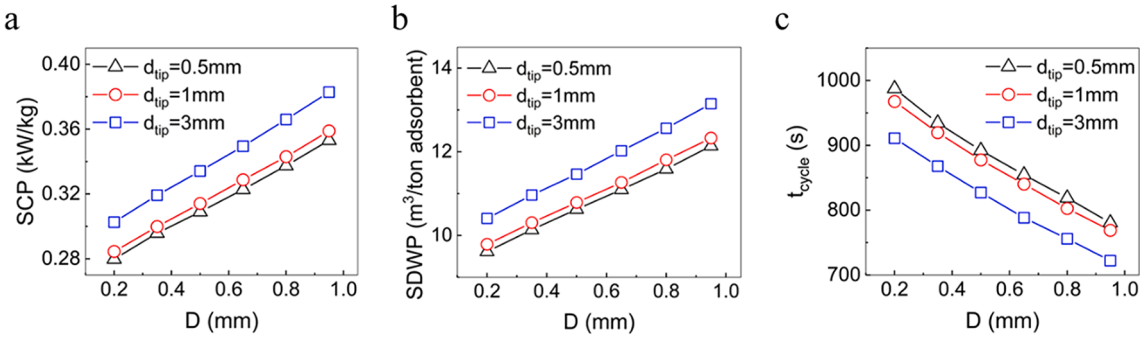

Fig. 6. Variations of (a) SCP, (b) SDWP, and (c) cycle time with the base diameter for different tip diameters.

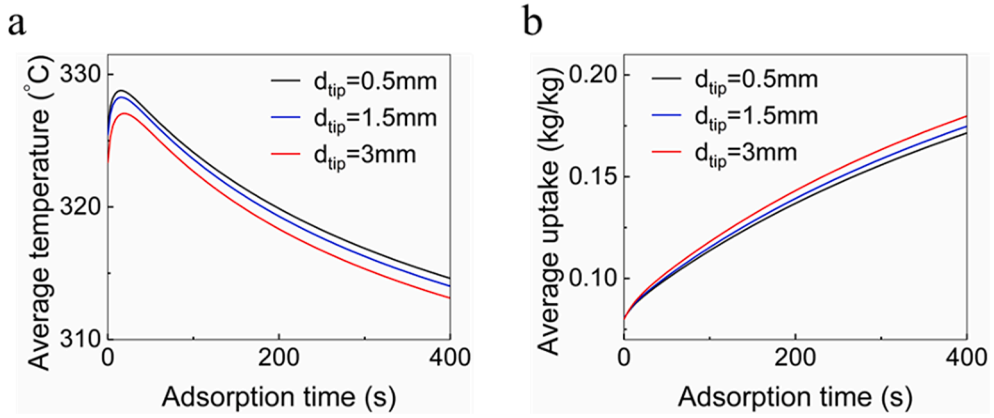

Fig. 7. Variations of (a) average temperature and (b) average uptake with adsorption time for different tip diameters. In the calculation, the base diameter and shape factor are fixed at 0.5 mm and 7, respectively.

nting the region with high temperature and low uptake, as depicted in Fig. 12. For the selected base and tip diameter which relatively has a large difference, the increase of shape factor makes the fin thickness varies rapidly, which means augmentation of the distance between the middle of the fins, as clearly shown in Fig. 12. As a result, the heat transfer in this area is weakened, deteriorating the adsorbent performance.

3.2. Bed consideration

To obtain the optimal fin shape for the system performance considering the whole bed, the TCP, TDWP and COP are furtherly investigated. The overall performances are calculated by integrating the uptake over the entire adsorbent area, thus the variation of adsorbent mass when changing the fin shape is considered and it can reflect the production and efficiency of the whole system.

3.2.1. The effect of base diameter

Fig. 13 presents the variations of total system performance with the base diameter for three fixed tip diameters. It can be observed from the figure that the production of cooling effect and freshwater almost monotonically decreases when the base diameter increases, which is just the opposite of the adsorbent performance discussed before. The adsorbent mass and average working capacity simultaneously impact the total system performance. Although the increase of base diameter causes an elevation of SCP and SDWP, the effect of the decrease of adsorbent mass due to more metal material employed is more predominant, leading to a reduction in cooling and water production. At the tip diameter of 0.5 mm, a base diameter of 0.35 mm leads to an optimal cooling effect of 0.151 kW and potable water production of 5.19 m^3 per day. This bed configuration primely balances the adsorbent mass and

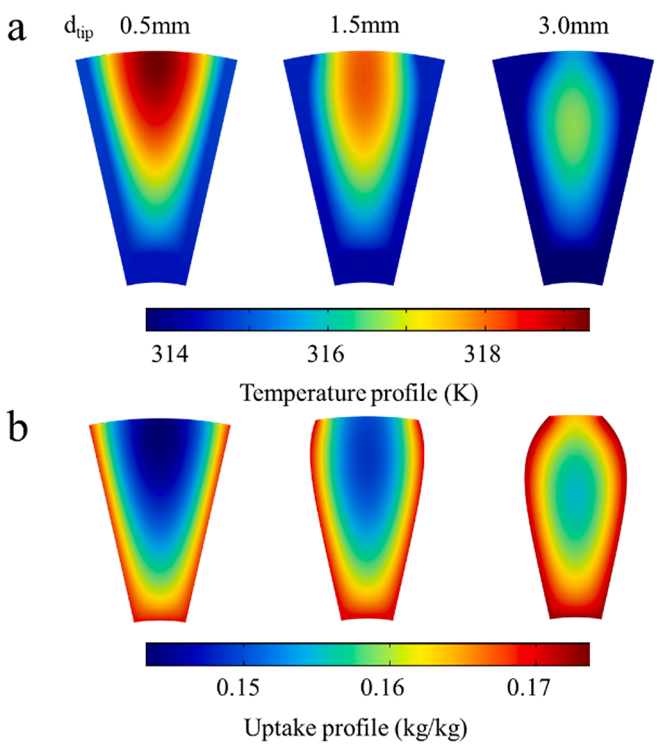

Fig. 8. (a) Temperature and (b) uptake distributions for the cross-sectional bed plain (the cross-section 10 mm from the surface) with fin dimensions of $D = 0.5$ mm, $H/l = 7$ and $d_{tip} = 0.5$ mm, 1.5 mm, 3.0 mm at 300 s of the isobaric adsorption process.

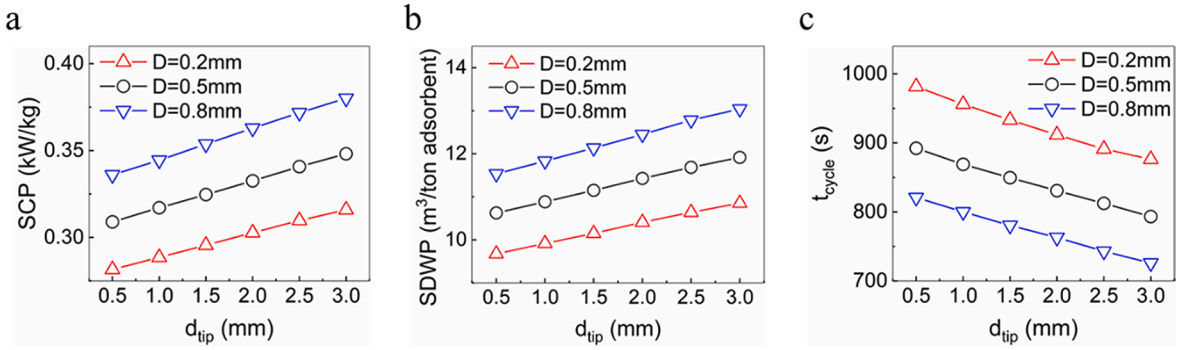

Fig. 9. Variations of (a) SCP, (b) SDWP, and (c) cycle time with the tip diameter for different base diameters. In the calculation, the shape factor is fixed at 7.

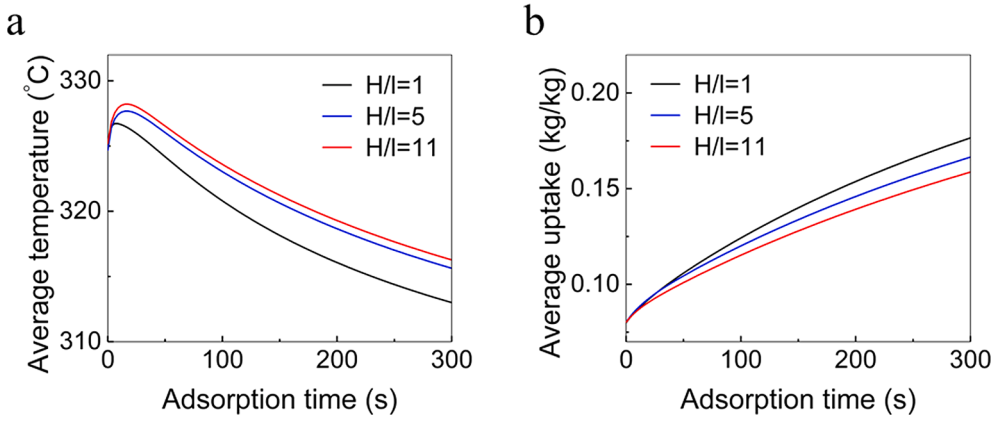

Fig. 10. Variations of (a) average temperature and (b) average uptake with adsorption time for different shape factors. In the simulation, the base and tip diameter are fixed at 0.5 mm and 2 mm, respectively.

heat transfer enhancement.

The coefficient of performance is examined in Fig. 13(c) at a constant shape factor of 11. It can be observed from the figure that the COP monotonically decreases with the augmentation of base diameter. Based on the expression presented in Table 1, the COP is calculated as the ratio of the cooling effect produced in the adsorption phase and the total supplied heat during desorption and preheating, which is partly consumed for the elevation of thermal energy of the fin, tube, and adsorbent and partially for the supply of latent desorption heat. Evidently, the increase of base diameter accounts for an augment of the energy used for the metal heating up and a reduction of latent desorption heat consumption, which is more significant, hence the decrease of the proportion of the energy consumed for desorption leads to the reduction of COP.

3.2.2. *The effect of tip diameter*

As presented in Fig. 14(a) and (b), the total cooling effect and freshwater throughput decrease along with the augment of tip diameter, especially for the bed configuration with a larger base diameter, which arises due to the rapid reduction of adsorbent mass in this situation. With a tip and base diameter fixed at 0.5 mm and 0.2 mm, respectively, the system produces the highest cooling effect of 0.151 kW and potable

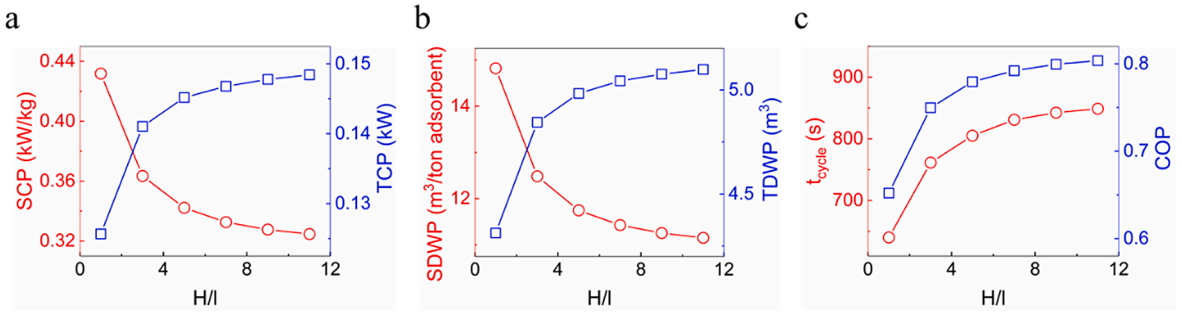

Fig. 11. Variations of (a) SCP and TCP, (b) SDWP and TDWP, (c) cycle time and COP with the shape factor. In the simulation, the base and tip diameter are fixed at 0.5 mm and 2 mm, respectively.

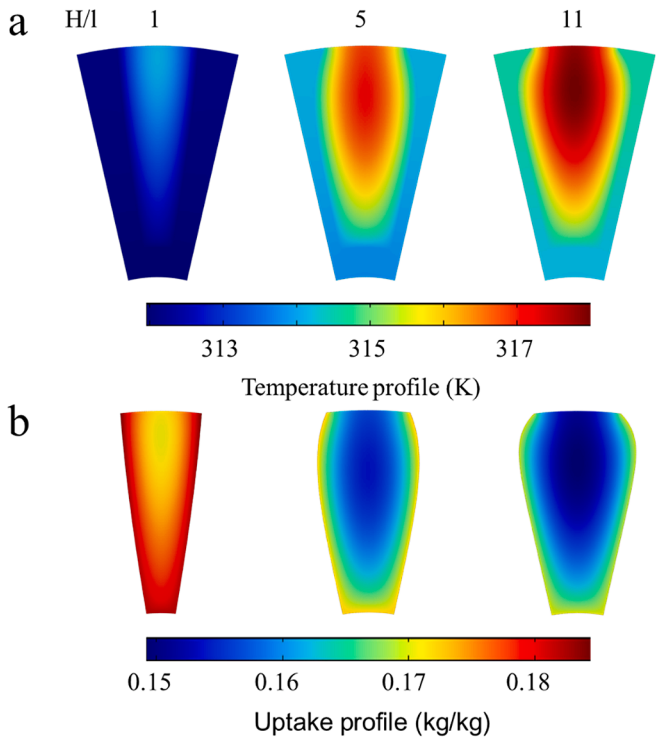

Fig. 12. (a) Temperature and (b) uptake distributions for the cross-sectional bed plain (the cross-section 10 mm from the surface) with fin dimensions of $D = 0.5$ mm, $d_{tip} = 2$ mm, and $H/l = 1$, 5, 11 at 300 s of the isobaric adsorption process.

water of 5.19 m^3 per day. Although the total throughput varies monotonically with the tip diameter, it does not mean the smallest tip diameter is optimal for the system. Indeed, the strong contradiction between the variations of specific parameters and the overall factors reveals that the optimal tip diameter is acquired when it balances the heat transfer enhancement and the adsorbent mass. Additionally, it can be observed from Fig. 14(c) that a larger tip diameter results in a lower COP, for which the elucidation is similar to the base diameter. The reduction of the proportion of desorption heat in the total supplied energy results in a decrease in COP. It reveals that the improvement of specific production generally companies with a slight cost of COP.

3.2.3. The effect of shape factor

The variations of total performance considering the whole bed with the fin shape factor are depicted in Fig. 11. The results reveal that at a base diameter of 0.5 mm and a tip diameter of 2 mm, the system throughput is improved along with the increase of shape factor, still opposed to the adsorbent performance. This discrepancy arises due to the augment of adsorbent mass when increasing the shape factor, which compensates for the heat transfer deterioration. It is also worth emphasizing that this conclusion merely applies to the umbrella-shaped fins which have a large gap between the tip and base diameter. Moreover, it can be observed from Fig. 11(c) that the COP monotonically increases as H/l augments, which is attributed to the enhancement of desorption. The aforementioned analysis illustrates a dramatic difference between the specific and total performance, which is caused by the predominant adsorbent mass under the relatively compact simulated geometrical characteristics. The results can also derive from many rectangular fin studies as inserting more metal material must lead to a reduction of adsorbent mass. However, the advantage of the application of irregular fins advanced in the study is that the variable fin thickness makes the reduction of adsorbent mass controllable. It reveals that the adsorbent particles in the regions presenting low specific performances can be precisely dislodged and replaced with metal. As presented in Fig. 15, the overall performances of the bed with irregular fins are compared with the adsorber with rectangular fins which has the same fin cross-sectional area. It clearly demonstrates the superiority of the advanced umbrella-shaped fins as it shows the higher TCP and TDWP than the conventional bed.

3.3. Machine learning and optimization

In the aforementioned analysis, three parameters manipulating the fin shape (base diameter, tip diameter, shape factor) are selected and their effect on the performance considering the adsorbent and the bed is comprehensively explored. There exist optimal fin parameters leading to the maximum total water production. To explore the optimal fin shape configuration for the total system performance, a machine learning method and genetic algorithm are employed and the procedure is listed in Fig. 17 (a). 216 cases are selected and numerically calculated, after post-processing steps, the total performances incorporating TCP, TDWP, and COP for each of the configurations can be derived and used for the machine learning step.

The machine learning process is conducted via ensemble-based models. The models are trained several times employing 5-fold cross-validation to alleviate the random error and derive the hidden quantitative relationship between the fin parameters and the total performance. Root mean square error (RMSE), R^2, mean absolute error (MAE), and mean square error (MSE) are applied to measure the accuracy of the models predicting the three total performance factors, for which the results are summarized in Table 4. The trained models are subsequently used for predicting the total performance parameters under each fin shape, and great accordance has been encountered, as presented in Fig. 16.

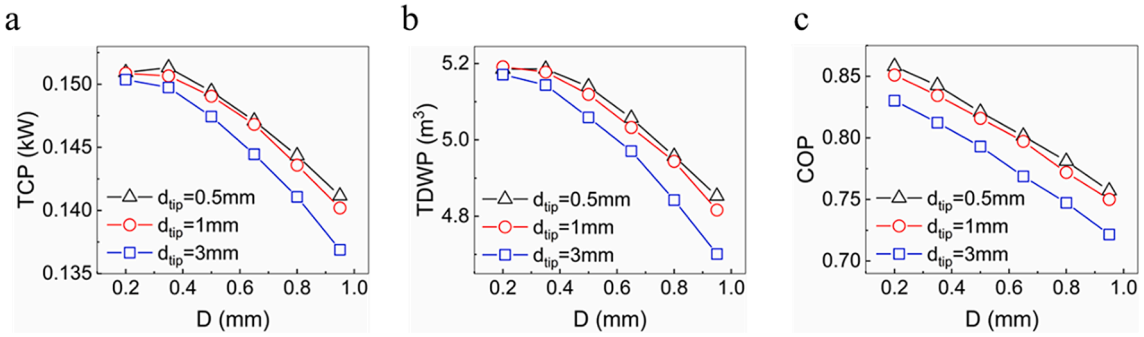

Fig. 13. Variations of (a) TCP, (b) TDWP, and (c) COP with the base diameter for different tip diameters. In the calculation, the shape factor is fixed at 11.

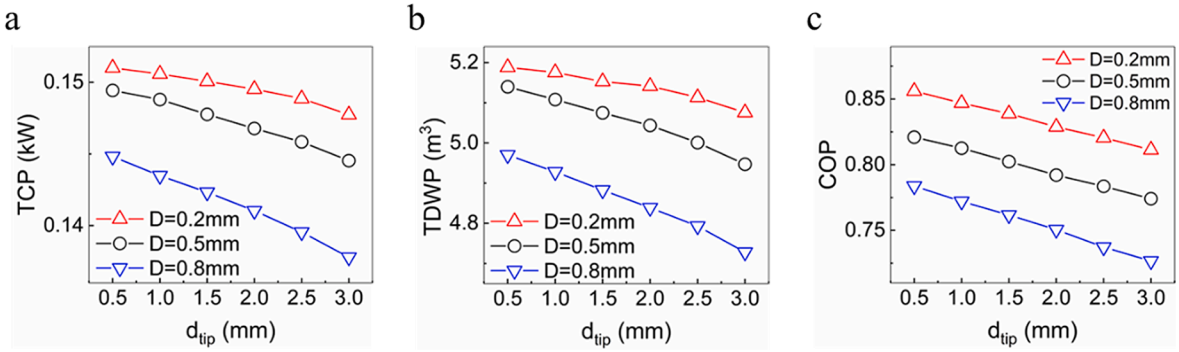

Fig. 14. Variations of (a) TCP, (b) TDWP, and (c) COP with the tip diameter for different base diameters. In the calculation, the shape factor is fixed at 7.

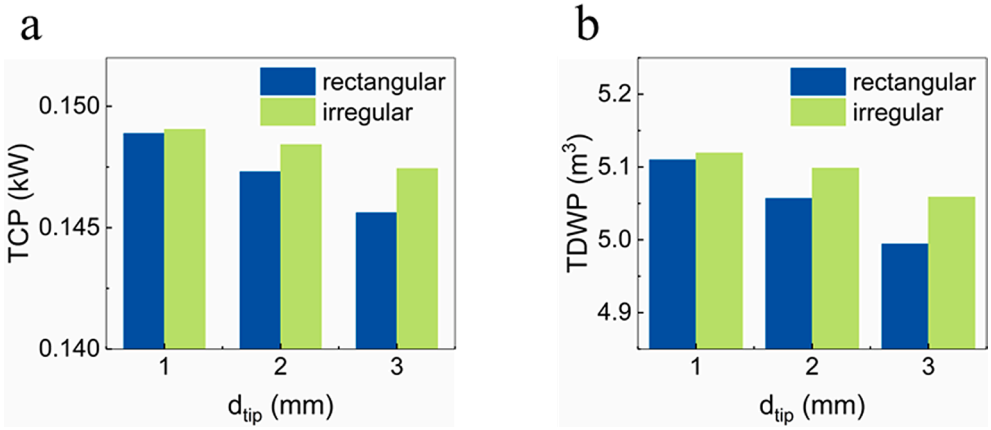

Fig. 15. Comparisons of (a) TCP and (b) TDWP between the bed with rectangular fins and irregular fins. In the simulation, the base diameter and shape factor are fixed at 0.5 mm and 11.

Considering the significant position of water production in the adsorption-based desalination and cooling systems, only the model of TDWP is employed in the genetic algorithm to acquire the optimal fin parameters for water production. The results illustrate that a fin shape with the base diameter, tip diameter, and shape factor fixed at 0.262, 0.517, and 4.20, respectively, leads to a maximum total water production of 5.20 m^3 per day with a relatively superior TCP of 0.149 kW and COP of 0.855. The optimization results reveal that the bed with umbrella-shaped fins presents better performance than that of the bullet-shaped or rectangular. It may arise due to the fact that the adsorbent particles with low working capacity and specific performance concentrate on the regions away from the tube wall, which is reduced in the bed with umbrella-shaped fins.

In addition, an alternative manner of balancing the adsorbent mass and heat transfer enhancement via the adjustment of L_1/L in discontinuous fins is investigated, where L_1 is the length of the fin and L is the total length of the periodic unit, as depicted in Fig. 17(b). It can be observed from Fig. 18 that increasing L_1/L almost leads to all the performance parameters, whether for adsorbent or bed, monotonically augmenting, which is fairly different from the factors examined aforementioned. This discrepancy may arise since the region with no fins has such a poor heat transfer efficiency thus an extremely deteriorated uptake that the adsorbent mass becomes subordinate while the heat transfer enhancement gets predominant.

4. Conclusion

Unlike traditional rectangular fins for finned-tube adsorbent bed in the AD system, irregular fins (bullet- or umbrella-shaped fin configurations) are employed in this paper. Based on a complete transient mathematical model that incorporates a three-dimensional computational fluid dynamic model for adsorbent bed and lumped models for evaporator and condenser, the effects of base diameter, tip diameter, and shape factor on system performances considering the adsorbent and the whole bed are comprehensively analyzed. The underlining relationship between fin configurations and overall system performance is further explored via machine learning. And the optimal fin configurations are identified by the genetic algorithm. General findings with respect to the optimization of bed configuration are listed below:

- The bed with umbrella-shaped fins renders better overall performance than the bullet-shaped ones and the traditional rectangular ones.
- Fin shape factors can be optimized to derive the maximum total system throughput.
- The optimal base diameter, tip diameter, and shape factor are 0.262, 0.517, and 4.20, respectively, which render a total water production of 5.20 m^3/day with a total cooling power of 0.149 kW and coefficient of performance of 0.855.
- The increase of L_1/L for discontinuous fins contributes to the specific and total system throughput. Therefore continuous fins are more appealing in practical applications.

Table 4
Accuracy of the machine learning models.

Trained factor	RSME	R^2	MSE	MAE
TCP	0.0022062	0.97	0.0000048673	0.0019469
TDWP	0.056569	0.98	0.0032	0.035226
COP	0.0097546	0.99	0.000095153	0.0056263

CRediT authorship contribution statement

Mingliang Li: Writing – original draft. **Yanan Zhao:** Visualization. **Rui Long:** Conceptualization, Writing – review & editing. **Zhichun Liu:** Investigation. **Wei Liu:** Formal analysis.

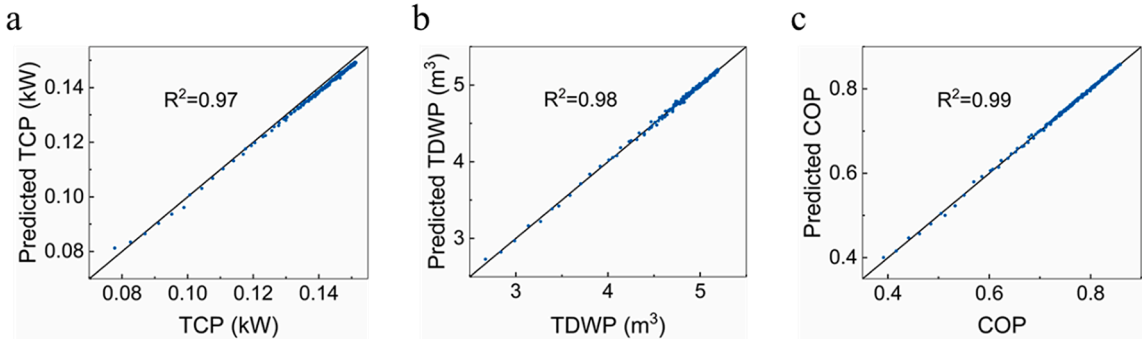

Fig. 16. Comparisons between predicted and calculated (a) TCP, (b) TDWP, and (c) COP during the ensemble-based machine learning process.

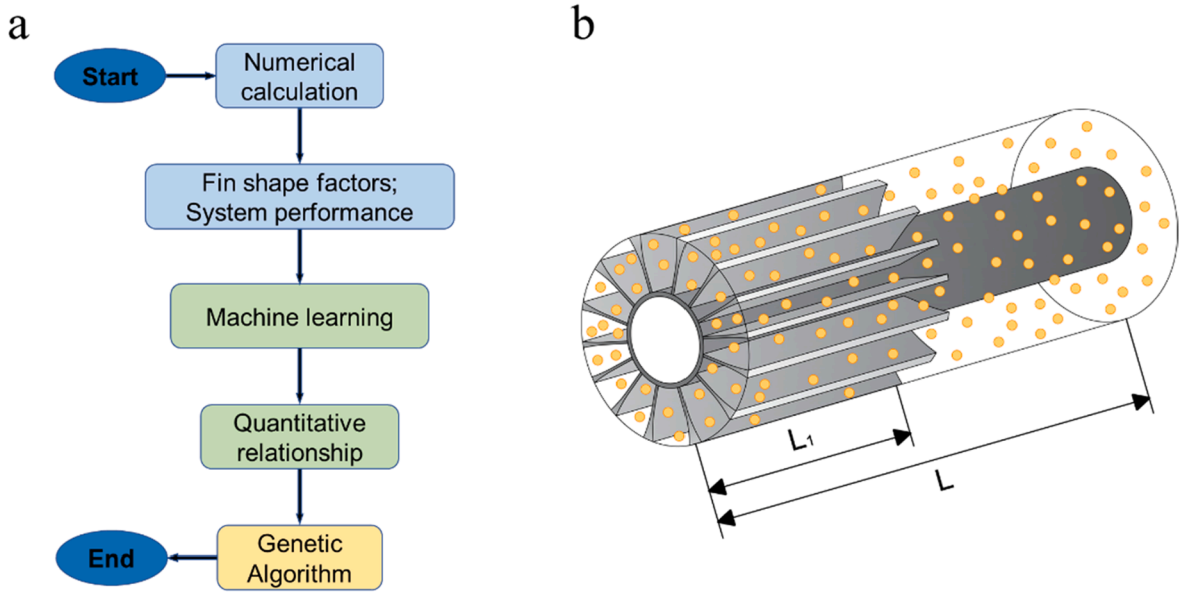

Fig. 17. (a) Flow chart for the machine learning procedure. (b) Schematic of the discontinuous fin.

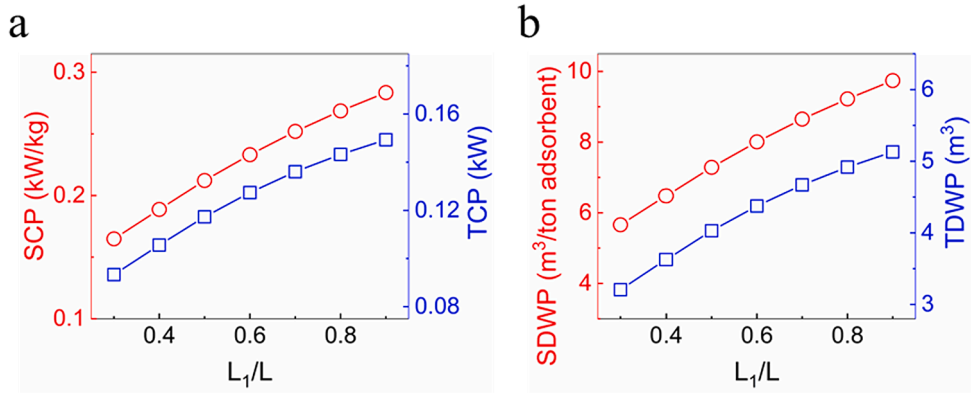

Fig. 18. Variations of (a) SCP and TCP, (b) SDWP and TDWP with the dimensionless length L_1/L.

Declaration of Competing Interest

The authors declare that they have no known competing financial interests or personal relationships that could have appeared to influence the work reported in this paper.

Acknowledgment

This work was financially supported by the National Natural Science Foundation of China (52176070, 51736004).

References

[1] M.H. Khoshgoftar Manesh, P. Firouzi, S. Kabiri, A.M. Blanco-Marigorta, Evaluation of power and freshwater production based on integrated gas turbine, S-CO2, and ORC cycles with RO desalination unit, Energy Convers. Manage. 228 (2021), 113607.
[2] S. Kabiri, M.H. Khoshgoftar Manesh, M. Yazdi, M. Amidpour, New procedure for optimal solar repowering of thermal power plants and integration with MSF desalination based on environmental friendliness and economic benefit, Energy Convers. Manage. 240 (2021), 114247.
[3] K. Thu, Y.-D. Kim, G. Amy, W.G. Chun, K.C. Ng, A hybrid multi-effect distillation and adsorption cycle, Appl. Energy 104 (2013) 810–821.
[4] O.S. Burheim, F. Seland, J.G. Pharoah, S. Kjelstrup, Improved electrode systems for reverse electro-dialysis and electro-dialysis, Desalination 285 (2012) 147–152.
[5] E.S. Ali, R.H. Mohammed, N.A.A. Qasem, S.M. Zubair, A. Askalany, Solar-powered ejector-based adsorption desalination system integrated with a humidification-dehumidification system, Energy Convers. Manage. 238 (2021), 114113.
[6] K. Thu, H. Yanagi, B.B. Saha, K.C. Ng, Performance analysis of a low-temperature waste heat-driven adsorption desalination prototype, Int. J. Heat Mass Transf. 65 (2013) 662–669.
[7] K.C. Ng, K. Thu, S.J. Oh, L. Ang, M.W. Shahzad, A.B. Ismail, Recent developments in thermally-driven seawater desalination: energy efficiency improvement by hybridization of the MED and AD cycles, Desalination 356 (2015) 255–270.
[8] A. Askalany, E.S. Ali, R.H. Mohammed, A novel cycle for adsorption desalination system with two stages-ejector for higher water production and efficiency, Desalination 496 (2020), 114753.
[9] A. Askalany, A.S. Alsaman, M. Ghazy, R.H. Mohammed, R. Al-Dadah, S. Mahmoud, Experimental optimization of the cycle time and switching time of a metal organic framework adsorption desalination cycle, Energy Convers. Manage. 245 (2021), 114558.
[10] K. Thu, B.B. Saha, K.J. Chua, K.C. Ng, Performance investigation of a waste heat-driven 3-bed 2-evaporator adsorption cycle for cooling and desalination, Int. J. Heat Mass Transf. 101 (2016) 1111–1122.
[11] A.S. Alsaman, A.A. Askalany, K. Harby, M.S. Ahmed, Performance evaluation of a solar-driven adsorption desalination-cooling system, Energy. 128 (2017) 196–207.
[12] B.B. Saha, I.I. El-Sharkawy, M.W. Shahzad, K. Thu, L. Ang, K.C. Ng, Fundamental and application aspects of adsorption cooling and desalination, Appl. Therm. Eng. 97 (2016) 68–76.
[13] H. Zhang, H. Ma, S. Liu, H. Wang, Y. Sun, D. Qi, Investigation on the operating characteristics of a pilot-scale adsorption desalination system, Desalination 473 (2020), 114196.
[14] S.-Y. Woo, H.-S. Lee, H. Ji, D.-S. Moon, Y.-D. Kim, Silica gel-based adsorption cooling cum desalination system: Focus on brine salinity, operating pressure, and its effect on performance, Desalination 467 (2019) 136–146.
[15] H.J. Dakkama, P.G. Youssef, R.K. Al-Dadah, S. Mahmoud, Adsorption ice making and water desalination system using metal organic frameworks/water pair, Energy Convers. Manage. 142 (2017) 53–61.
[16] K. Thu, K.C. Ng, B.B. Saha, A. Chakraborty, S. Koyama, Operational strategy of adsorption desalination systems, Int. J. Heat Mass Transf. 52 (7–8) (2009) 1811–1816.
[17] S. Mitra, P. Kumar, K. Srinivasan, P. Dutta, Performance evaluation of a two-stage silica gel + water adsorption based cooling-cum-desalination system, Int. J. Refrig. 58 (2015) 186–198.
[18] M. Li, Y. Zhao, R. Long, Z. Liu, W. Liu, Gradient porosity distribution of adsorbent bed for efficient adsorption cooling, Int. J. Refrig. 128 (2021) 153–162.
[19] S. Jribi, T. Miyazaki, B.B. Saha, S. Koyama, S. Maeda, T. Maruyama, Corrected adsorption rate model of activated carbon–ethanol pair by means of CFD simulation, Int. J. Refrig. 71 (2016) 60–68.
[20] M.M. Abd-Elhady, A.M. Hamed, Effect of fin design parameters on the performance of a two-bed adsorption chiller, Int. J. Refrig. 113 (2020) 164–173.
[21] S. Mitra, N. Aswin, P. Dutta, Scaling analysis and numerical studies on water vapour adsorption in a columnar porous silica gel bed, Int. J. Heat Mass Transf. 95 (2016) 853–864.
[22] T. Miyazaki, A. Akisawa, B.B. Saha, I.I. El-Sharkawy, A. Chakraborty, A new cycle time allocation for enhancing the performance of two-bed adsorption chillers, Int. J. Refrig. 32 (5) (2009) 846–853.
[23] S.M. Ali, A. Chakraborty, Adsorption assisted double stage cooling and desalination employing silica gel + water and AQSOA-Z02 + water systems, Energy Convers. Manage. 117 (2016) 193–205.
[24] P.G. Youssef, S.M. Mahmoud, R.K. Al-Dadah, Performance analysis of four bed adsorption water desalination/refrigeration system, comparison of AQSOA-Z02 to silica-gel, Desalination 375 (2015) 100–107.
[25] P.G. Youssef, S.M. Mahmoud, R.K. Al-Dadah, Numerical simulation of combined adsorption desalination and cooling cycles with integrated evaporator/condenser, Desalination 392 (2016) 14–24.
[26] K. Thu, B.B. Saha, A. Chakraborty, W.G. Chun, K.C. Ng, Study on an advanced adsorption desalination cycle with evaporator–condenser heat recovery circuit, Int. J. Heat Mass Transf. 54 (1–3) (2011) 43–51.
[27] M. Mahdavikhah, H. Niazmand, Effects of plate finned heat exchanger parameters on the adsorption chiller performance, Appl. Therm. Eng. 50 (1) (2013) 939–949.
[28] E. Elsayed, R. Al-Dadah, S. Mahmoud, A. Elsayed, P.A. Anderson, Aluminium fumarate and CPO-27(Ni) MOFs: Characterization and thermodynamic analysis for adsorption heat pump applications, Appl. Therm. Eng. 99 (2016) 802–812.
[29] E. Elsayed, R. Al-Dadah, S. Mahmoud, P.A. Anderson, A. Elsayed, P.G. Youssef, CPO-27(Ni), aluminium fumarate and MIL-101(Cr) MOF materials for adsorption water desalination, Desalination 406 (2017) 25–36.
[30] A. Freni, G. Maggio, F. Cipitì, Y.I. Aristov, Simulation of water sorption dynamics in adsorption chillers: One, two and four layers of loose silica grains, Appl. Therm. Eng. 44 (2012) 69–77.
[31] Y.I. Aristov, Experimental and numerical study of adsorptive chiller dynamics: loose grains configuration, Appl. Therm. Eng. 61 (2) (2013) 841–847.
[32] G.G. Ilis, M. Mobedi, S. Ülkü, A dimensionless analysis of heat and mass transport in an adsorber with thin fins; uniform pressure approach, Int. Commun. Heat Mass Transfer 38 (6) (2011) 790–797.
[33] H. Niazmand, I. Dabzadeh, Numerical simulation of heat and mass transfer in adsorbent beds with annular fins, Int. J. Refrig 35 (3) (2012) 581–593.
[34] M. Mohammadzadeh Kowsari, H. Niazmand, M.M. Tokarev, Bed configuration effects on the finned flat-tube adsorption heat exchanger performance: numerical modeling and experimental validation, Appl. Energy 213 (2018) 540–554.
[35] M.M. Saleh, R. Al-Dadah, S. Mahmoud, E. Elsayed, O. El-Samni, Wire fin heat exchanger using aluminium fumarate for adsorption heat pumps, Appl. Therm. Eng. 164 (2020), 114426.
[36] M. Li, Y. Zhao, R. Long, Z. Liu, W. Liu, Computational fluid dynamic study on adsorption-based desalination and cooling systems with stepwise porosity distribution, Desalination 508 (2021), 115048.
[37] M. Li, Y. Zhao, R. Long, Z. Liu, W. Liu, Field synergy analysis for heat and mass transfer characteristics in adsorption-based desalination and cooling systems, Desalination 517 (2021), 115244.
[38] M.B. Elsheniti, M.A. Hassab, A.-E. Attia, Examination of effects of operating and geometric parameters on the performance of a two-bed adsorption chiller, Appl. Therm. Eng. 146 (2019) 674–687.
[39] J.W. Wu, M.J. Biggs, E.J. Hu, Dynamic model for the optimisation of adsorption-based desalination processes, Appl. Therm. Eng. 66 (1–2) (2014) 464–473.
[40] R.H. Mohammed, O. Mesalhy, M.L. Elsayed, M. Su, C.L. Chow, Revisiting the adsorption equilibrium equations of silica-gel/water for adsorption cooling applications, Int. J. Refrig. 86 (2018) 40–47.
[41] K. Thu, A. Chakraborty, Y.-D. Kim, A. Myat, B.B. Saha, K.C. Ng, Numerical simulation and performance investigation of an advanced adsorption desalination cycle, Desalination 308 (2013) 209–218.
[42] H.T. El-Dessouky, H.M. Ettouney, Fundamentals of Salt Water Desalination, Elsevier Science B.V., 2020.
[43] D. Cheng, E.A.J.F. Peters, J.A.M. Kuipers, Performance study of heat and mass transfer in an adsorption process by numerical simulation, Chem. Eng. Sci. 160 (2017) 335–345.
[44] F.N. Al-Mousawi, R. Al-Dadah, S. Mahmoud, Different bed configurations and time ratios: performance analysis of low-grade heat driven adsorption system for cooling and electricity, Energy Convers. Manage. 148 (2017) 1028–1040.
[45] İ. Solmuş, S. Andrew, D. Rees, C. Yamalı, D. Baker, A two-energy equation model for dynamic heat and mass transfer in an adsorbent bed using silica gel/water pair, Int. J. Heat Mass Transf. 55 (19–20) (2012) 5275–5288.
[46] R.H. Mohammed, A simplified method for modeling of round and square ceiling diffusers, Energy Build. 64 (2013) 473–482.
[47] M.A. Aziz, I.A.M. Gad, E.S.F.A. Mohammed, R.H. Mohammed, Experimental and numerical study of influence of air ceiling diffusers on room air flow characteristics, Energy Build. 55 (2012) 738–746.
[48] A. Sapienza, S. Santamaria, A. Frazzica, A. Freni, Influence of the management strategy and operating conditions on the performance of an adsorption chiller, Energy. 36 (9) (2011) 5532–5538.
[49] Y.I. Aristov, A. Sapienza, D.S. Ovoshchnikov, A. Freni, G. Restuccia, Reallocation of adsorption and desorption times for optimisation of cooling cycles, Int. J. Refrig. 35 (3) (2012) 525–531.
[50] M. Li, Y. Zhao, R. Long, Z. Liu, W. Liu, Metal foam packed adsorbent bed boosting the performance of the adsorption-based desalination and cooling system, Energy Convers. Manage. 254 (2022).
[51] R.H. Mohammed, O. Mesalhy, M.L. Elsayed, L.C. Chow, Performance evaluation of a new modular packed bed for adsorption cooling systems, Appl. Therm. Eng. 136 (2018) 293–300.
[52] R.H. Mohammed, O. Mesalhy, M.L. Elsayed, L.C. Chow, Scaling analysis of heat and mass transfer processes in an adsorption packed bed, Int. J. Therm. Sci. 133 (2018) 82–89.
[53] R.H. Mohammed, O. Mesalhy, M.L. Elsayed, L.C. Chow, Assessment of numerical models in the evaluation of adsorption cooling system performance, Int. J. Refrig. 99 (2019) 166–175.